JOURNAL OF SOLID STATE CHEMISTRY 73, 107–117 (1988)

$BaMn_{1-x}Fe_xO_{3-\delta}$, An Oxygen-Deficient 6H′ Oxide: Electron Microscopy, Powder Neutron Diffraction, and Mössbauer Study

V. CAIGNAERT,* M. HERVIEU, B. DOMENGÈS, N. NGUYEN, J. PANNETIER,† AND B. RAVEAU

Laboratoire de Cristallographie, Chimie et Physique des Solides, U.A. 251, ISMRa-Université, 14032 Caen Cedex, France, and †Institut Max Von Laue-Paul Langevin, 156X Centre de Tri, 38042 Grenoble Cedex, France

Received January 15, 1986; in revised form April 17, 1986

A rather rare six-layer form of "hexagonal perovskite" 6H′, was isolated for $BaMn_{1-x}Fe_xO_{3-\delta}$ ($0 \leq x \leq 0.3$). X-ray powder diffraction and HREM studies have shown that the stacking sequence of the BaO_3 layers is *hhhchc*. The distributions of oxygen vacancies and octahedral cations were determined by powder neutron diffraction for $x = 0.233$. The coordination of iron ions was determined by Mössbauer spectroscopy. © 1988 Academic Press, Inc.

Introduction

The consideration of the perovskite structure AMO_3 along the ⟨111⟩ direction of the cubic cell leads to a description of this structure in terms of an *a b c* close-packing of AO_3 layers forming octahedral cavities where the *M* ions are located. Numerous stoichiometric oxides AMO_3, called "hexagonal perovskites" (*1–2*), exhibit a structure related to the perovskite since they are characterized by a close-packing of AO_3 layers forming octahedral cavities, but differ greatly from the true perovskite structure by the nature of the stacking of the AO_3 layers. Consequently, the distribution of the *M* ions in the octahedral holes is very different from the perovskite involving the presence of face-sharing MO_6 octahedra instead of corner-sharing octahedra. When the *M* element is able to take simultaneously several oxidation states and coordinations, oxygen-deficient AMO_{3-x} oxides can be synthesized; this phenomenon, which has been observed for the barium oxides $BaMO_{3-x}$ (*M* = Fe, Mn, CO) (*3–9*), is very complex: the relationships between the range of nonstoichiometry in these phases and the stacking sequences has not been explained up to the present. This lack of knowledge results from the difficulty in locating the oxygen vacancies in the structure. The distribution of oxygen vacancies in those structures has been determined by powder neutron diffraction for only few oxides: 12H $BaCoO_{2.6}$ (*8*) 6H $BaFeO_{2.79}$ (*4*), and 4H $Ba_{1/2}Sr_{1/2}MnO_{2.84}$ (*10*).

A rather rare six-layer form has been isolated in the system $BaMnO_{3-\delta}$ for δ ranging from 0.10 to 0.15 (*3*). The X-ray powder diffraction study of this phase has shown that the stacking sequence of the BaO_3 layers is *hchhhc*, whereas the commonly en-

Present address: U.A. 251, ISMRa-Université, 14032 Caen Cedex, France.

0022-4596/88 $3.00

countered sequence in 6H oxides is $(hcc)_2$ (see, for instance, $BaTiO_3$ (*11*), $BaFeO_{3-x}$ (*4*), and $BaCrO_{3-x}$ (*12*)). The comparison between the $BaMnO_{3-\delta}$ and $BaFeO_{3-x}$ systems shows that a structure, which will be denoted as 6H′ is favored by the presence of manganese. To understand the role of manganese and oxygen nonstoichiometry in the stabilization of the 6H′ structure, the study of the substitution of iron by manganese in the $BaMnO_{3-\delta}$ system was undertaken. The present work deals with the structural study of the oxygen deficient 6H′ oxide $BaMn_{1-x}Fe_xO_{3-\delta}$ ($0 \leq x \leq 0.3$).

Experimental

Synthesis and chemical analysis. Mixtures of $BaCO_3$, Mn_3O_4, and Fe_2O_3 were heated at 1100°C in air to ensure decarbonation and then heated at 1300°C in air for 3 days.

The oxygen content was determined by chemical analysis: the oxide was dissolved in an hydrochloric acid solution with an excess of titrated ferrous solution; the excess of Fe^{2+} was then back-titrated with $K_2Cr_2O_7$. The oxygen content could thus be determined, assuming that iron is trivalent and manganese is bivalent in the presence of excess Fe^{2+}.

Crystallographic study. The powder patterns were obtained with a Philips diffractometer using Cu$K\alpha$ radiation. Unit cell parameters were calculated using a least-squares program. The electron diffraction data used for the determination of the crystal symmetry and the reflection conditions were recorded by means of a Jeol 100CX microscope fitted with an eucentric side-entry goniometer (±60°) and operated at 120 kV. The microscopy samples were obtained from the polycrystalline sinters by crushing and dispersing in alcohol on carbon-coated grids.

The HREM study was carried out with a double-tilt top-entry goniometer (±10°) with a high resolution objective lens (spherical aberration constant of 0.7 mm). The objective aperture radius was of 0.42 $Å^{-1}$ in reciprocal space and the beam divergence was about 1.10^{-3} rad.

Neutron diffraction study. Neutron diffraction data were collected at room temperature at the diffractometer D1B of the Laue-Langevin Institute. The sample was contained in a thin-vanadium can and the wavelength was 2.5185 Å. Data were collected in the range $4° < \theta < 70°$ in two steps.

Integrated intensities were obtained by fitting the shape of the Bragg peaks to Gaussian and background to a first- or second-order polynomial. Neutron scattering lengths were taken as: $f_{Ba} = 52.8$, $f_{Mn} = -37.3$, $f_{Fe} = 95.4$, $f_O = 58.05$.

Magnetic study. ^{57}Fe Mössbauer spectra were recorded at room temperature using a ^{57}Co source in a rhodium host. Spectra were fitted with the Mosfit program developed by F. Varret and J. Teillet (*21*). The magnetic susceptibility was measured with a Faraday balance in the range of temperature: 4–600 K.

Results and Discussion

Crystallographic Data

The 6H′-form $BaMn_{1-x}Fe_xO_{3-\delta}$ has been isolated for a rather wide homogeneity range: $0 \leq x \leq 0.30$. One observes (Table I) that for the same experimental method, the

TABLE I

CHEMICAL ANALYSIS RESULTS: $BaMn_{1-x}Fe_xO_{3-\delta}$

x	δ	$M^{4+}(\%)/M^{3+}(\%)$
0.167	0.109(1)	78.2/21.8
0.233	0.129(1)	74.2/25.8
0.300	0.177(1)	64.6/35.4

TABLE II

CRYSTALLOGRAPHIC DATA: $BaMn_{1-x}Fe_xO_{3-\delta}$, HEXAGONAL CELL

x	a (Å)	c (Å)	V (Å^3)	$c/6a$
0.000	5.657(1)	13.997(2)	387.9(2)	0.4124(3)
0.050	5.662(1)	14.028(1)	389.5(2)	0.4129(2)
0.100	5.672(1)	14.063(7)	391.8(3)	0.4132(7)
0.167	5.687(1)	14.112(5)	393.7(3)	0.4144(5)
0.233	5.687(2)	14.167(4)	396.8(4)	0.4152(6)
0.300	5.706(2)	14.243(4)	401.6(4)	0.4160(6)

oxygen content decreases as x increases, from $\delta = 0$ for $x = 0$ to $\delta = 0.177$ for $x = 0.30$. This is in agreement with the replacement of Mn(IV) by Fe(III) in the structure. It is worth noting that by increasing the temperature of synthesis, greater oxygen deficiency can be induced: the heating of $BaMnO_{2.9}$ at 1470°C leads to $BaMnO_{2.86}$ previously isolated by Negas and Roth (*3*).

The lattice parameters increase with x (Table II) in agreement with the replacement of the Mn(IV) ions by Fe(III) ions of greater size. In the same way, the greater parameters of the more oxygen deficient oxide $BaMnO_{2.86}$ result from the replacement of Mn(IV) ions by Mn(III) ions.

All the crystals examined by electron diffraction exhibit a "c" parameter characteristic of a 6-layer stacking, the absence of systemic extinction leads to the space group $P\bar{6}m2$, previously proposed for $BaMnO_{2.90}$ (*3*). Previous studies showed that images from correctly oriented thin crystals could be correlated with the stacking of the BaO_3 layers in perovskite-related phase (*8, 13–18*). The projections of several 6-layer sequences were compared with the lattice image shown in Fig. 2 and 4; it appears clearly that a good agreement is observed with the sequence *hchhhc* (see under HREM study). An idealized drawing of 6H′-structure is shown in Fig. 1.

A preliminary structure calculation from X-ray powder data confirms the original 6H′ sequence, similar to that observed for $BaMnO_{2.90}$. The X-ray reflection intensities were measured by means of a planimeter and entered in a computer program taking into account the overlapping reflections. In the refinement, the atomic scattering factors for Ba^{2+}, Mn^{4+}, Fe^{3+}, and O^{2-}, given by Cromer and Waber were corrected for the anomalous dispersion. In spite of the low $R_I = \Sigma|I_o - I_c|/\Sigma I_o$ factor ($R_I < 0.10$), the numerous oxygen atoms of the structure, and the distribution of the oxygen vacancies could not be determined by this method. Moreover, it was not possible to determine the distribution of the metallic ions, owing to the similar scattering factors of manganese and iron.

Structure calculations were thus performed from neutron diffraction data, using 28 reflections, i.e., 60 *hkl* for the composition $BaMn_{0.766}Fe_{0.233}O_{2.87}$. The starting atomic coordinates were taken as those corresponding to the ideal close-packing of the BaO_3 layers in the sequence *hchhhc*; the distribution of the manganese and iron atoms was initially assumed to be random and the oxygen sites were taken as fully occupied.

Several refinements were carried out on the Mn/Fe distribution, atomic positions,

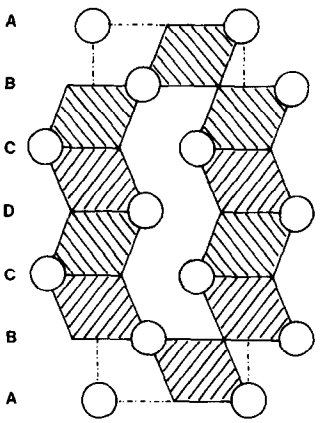

FIG. 1. Idealized drawing of 6H′ structure.

TABLE III

STRUCTURAL DATA OF COMPOUND: $BaMn_{0.767}Fe_{0.233}O_{2.87}$

At.	Site	x	y	z	B (Å^2)	T occupancy factor
Ba1	1(*a*)	0.000	0.000	0.000	0.8	1.00
Ba2	1(*d*)	0.333	0.667	0.500	1.0	1.00
Ba3	2(*h*)	0.333	0.667	0.178(2)	0.8	1.00
Ba4	2(*i*)	0.667	0.333	0.342(2)	0.9	1.00
M1	2(*g*)	0.000	0.000	0.243(6)	0.1	0.87/0.13(8)[a]
M2	2(*g*)	0.000	0.000	0.417(4)	1.2	0.98/0.02(3)[a]
M3	2(*i*)	0.667	0.333	0.113(3)	0.7	0.46/0.54(3)[a]
O1	3(*k*)	0.848(2)	0.696(4)	0.500	0.2	1.00
O2	3(*j*)	0.523(2)	0.046(4)	0.000	0.7	0.74(4)
O3	6(*n*)	0.836(1)	0.672(2)	0.166(1)	0.9	1.00
O4	6(*n*)	0.152(2)	0.304(4)	0.329(1)	0.3	1.00

[a] Mn/Fe.

oxygen occupancy factor and thermal factors, successively. The discrepancy factor calculated on the intensities was finally lowered to $R_I = 0.05$ ($R_I = \Sigma|I_o - I_c|/\Sigma I_o$). The atomic coordinates (Table III) are rather close to those observed by X-ray diffraction for $BaMn_{0.766}Fe_{0.233}O_{2.87}$.

HREM Study

The stacking sequences adopted by the perovskite-related phases, and the relationships with the ranges of non-stoichiometry when they are anion-deficient, are complex. These polytypes have been studied by high-resolution electron microscopy: the authors (*13–18*) demonstrated that the lattice images can be correlated with the stacking sequence of the BaO_3 layers, taking into account the dark rows of the barium ions in these images and the reversal of the slopes as witness of a hexagonal close-packed layer. For the study of $BaMn_{0.766}Fe_{0.233}O_{2.87}$, we have thus combined the different methods: the observation of the contrast of the lattice images permits a determination of the stacking sequence and then, the X-ray and neutron diffraction data were used to calculate the images.

Lattice images were obtained from suitably thin crystals oriented so that the electron beam was incident along $\langle 10\bar{1}0 \rangle$; astigmatism was corrected by observing the granularity of the support carbon film. A series of micrographs was taken over a range of defocus values from $\Delta f \sim 0$ to about 1000 Å. Simulated images were calculated using the multislice method and programs written by Skarnulis *et al.* (*19*), with the atomic coordinates of Table III.

In these images, even in the thinnest regions of the crystals rapid variations of the contrast were observed with thickness. On the thinnest edges, the contrast appears as an array of white blobs, whereas in the slightly thicker regions the images show an array of white and black chevrons. Enlarged images of Fig. 2 and 4, respectively, illustrate that feature.

The array of white and dark blobs observed in Fig. 2a in the thinnest edges of the crystal is in good agreement with the simulated image obtained for $\Delta f \sim 500$ Å and $15 < t < 30$ Å (Fig. 2b). Comparison with the projected potential shows that the dark blobs correspond to the barium atom positions; between these dark blobs (Mn and Fe) cation positions appear as less dark smears and the white dots correspond to the areas of slight projected charge density, near the oxygen positions. These images, clearly show one prominent row of white dots (perpendicularly to **c**), located between two less white ones. As previously observed in deficient $BaMO_{3-x}$ oxides (*14*) the oxygen does not contribute significantly to the image contrast so that the image is not affected by the oxygen vacancies (30% on O_2 atom) (Table III); our hypothesis was that this feature is correlated with the displacement of the M cations (M_3) (Table III), related to the oxygen vacancies, with regard to an ideal octahedral position. This hypothesis is in agreement with the simulated images shown, for example, in Fig. 3. These images were calculated for the same defocus and thickness values: (a) refined

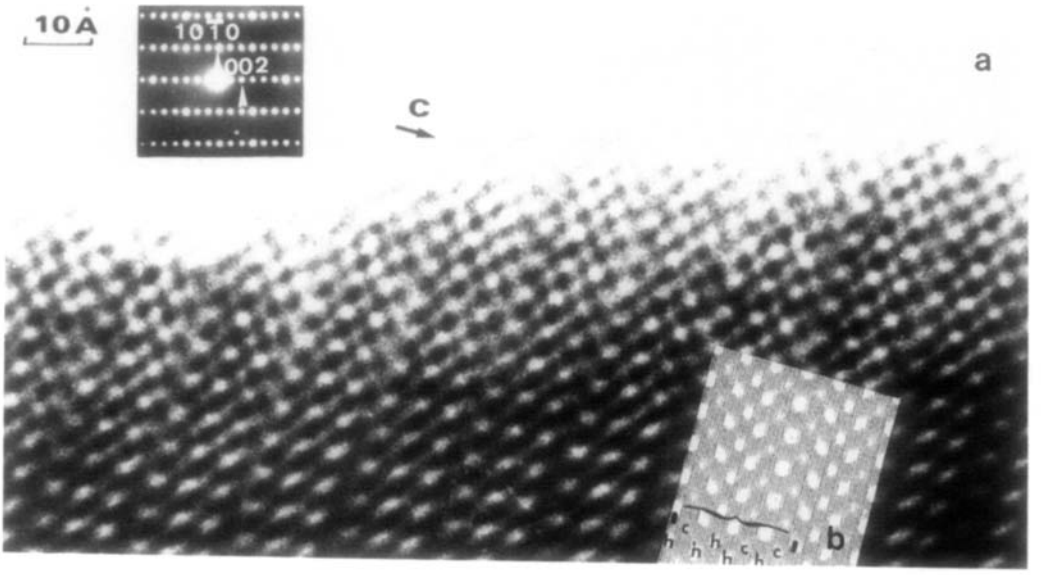

FIG. 2. High-resolution image of a thin edge of $BaMn_{0.766}Fe_{0.233}O_{2.87}$ in the $|10\bar{1}0|$ zone (a) and simulated image obtained for $\Delta f \sim 500$ Å and $t = 17.1$ Å (b).

atomic positions of M_3 with oxygen vacancies on O_2, (b) refined atomic position of M_3 without oxygen vacancies, and (c) M_3 cation in ideal (octahedral) position with oxygen vacancies and O_2.

For thicker regions the images display an array of alternating black and white chevrons, separated by approximately 5.6 Å and exhibiting four slope reversals (Fig. 4a), similar to those previously described (*14–16*); these images allow the *A*-site cations and stacking of the BaO_3 layers to be defined. To check this interpretation focus series were calculated: for $t \sim 85$ Å, they are shown in Fig. 4b. For $\Delta f \sim 600$ Å, it appears unambigously that the dark chevrons correspond to the column of barium and *M* cations and that the slope reversal indicates a h.c.p arrangement of the associated BaO_3 layer.

The high degree of ordering of the BaO_3 layers is noteworthy. During our investigations, only one stacking fault was observed (Fig. 5); it corresponds to 8-layer stacking, with a sequence *hchhhhhc*, different from that observed in the eight-layer $BaMnO_3$

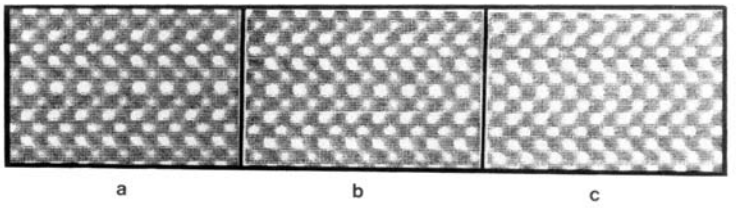

FIG. 3. Calculated images ($\Delta f = 500$ Å and $t = 17.1$ Å) obtained with (a) refined atomic position of M_3 with oxygen vacancies on O_2; (b) refined atomic position of M_3 without oxygen vacancies; and (c) M_3 cation in ideal octahedral position with oxygen vacancies on O_2.

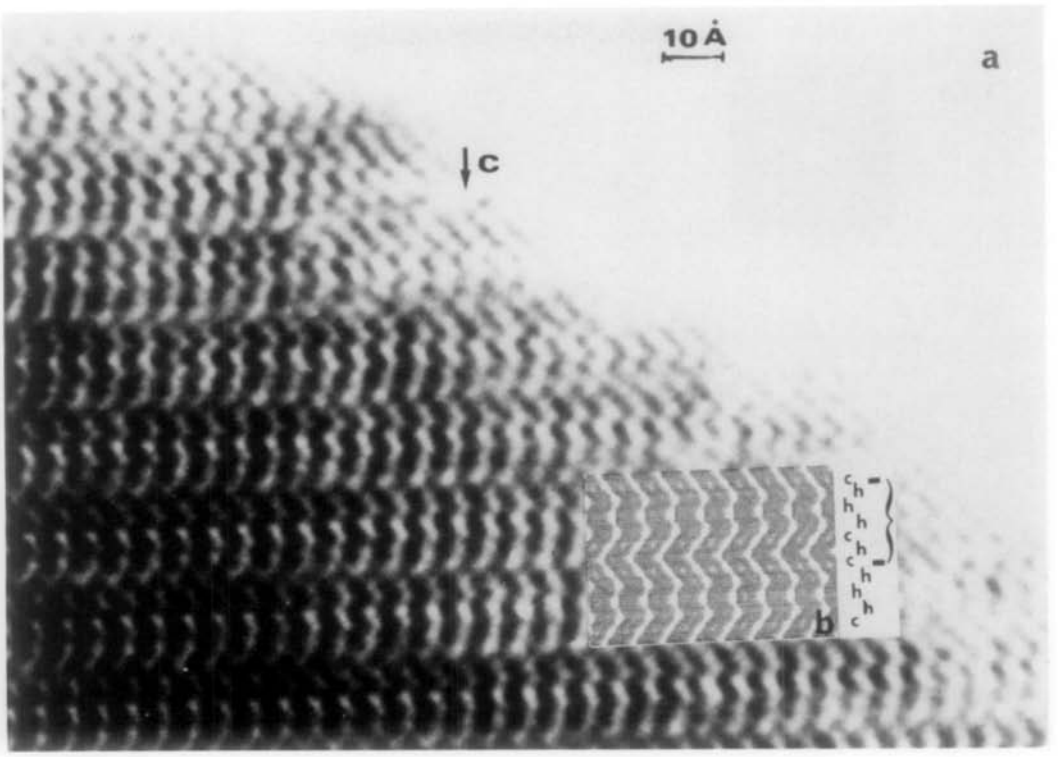

FIG. 4. High-resolution image of a thicker region and the calculated image ($\Delta f = 600$ Å, $t = 85.5$ Å).

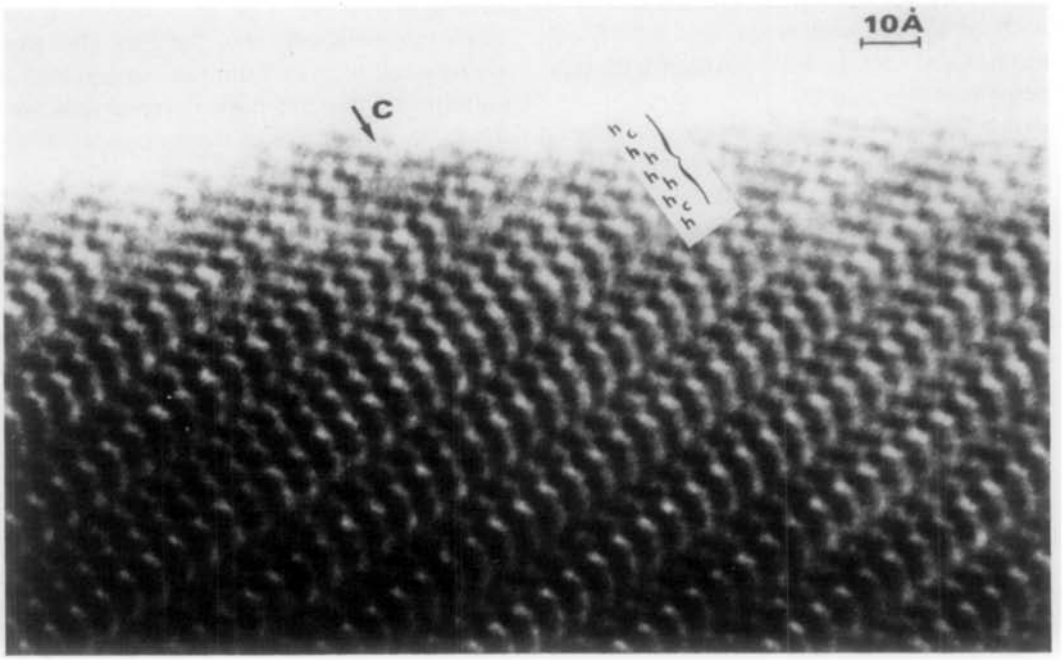

FIG. 5. Stacking fault observed in the matrix; it corresponds to a 8H stacking with a sequence *hchhhhhc*.

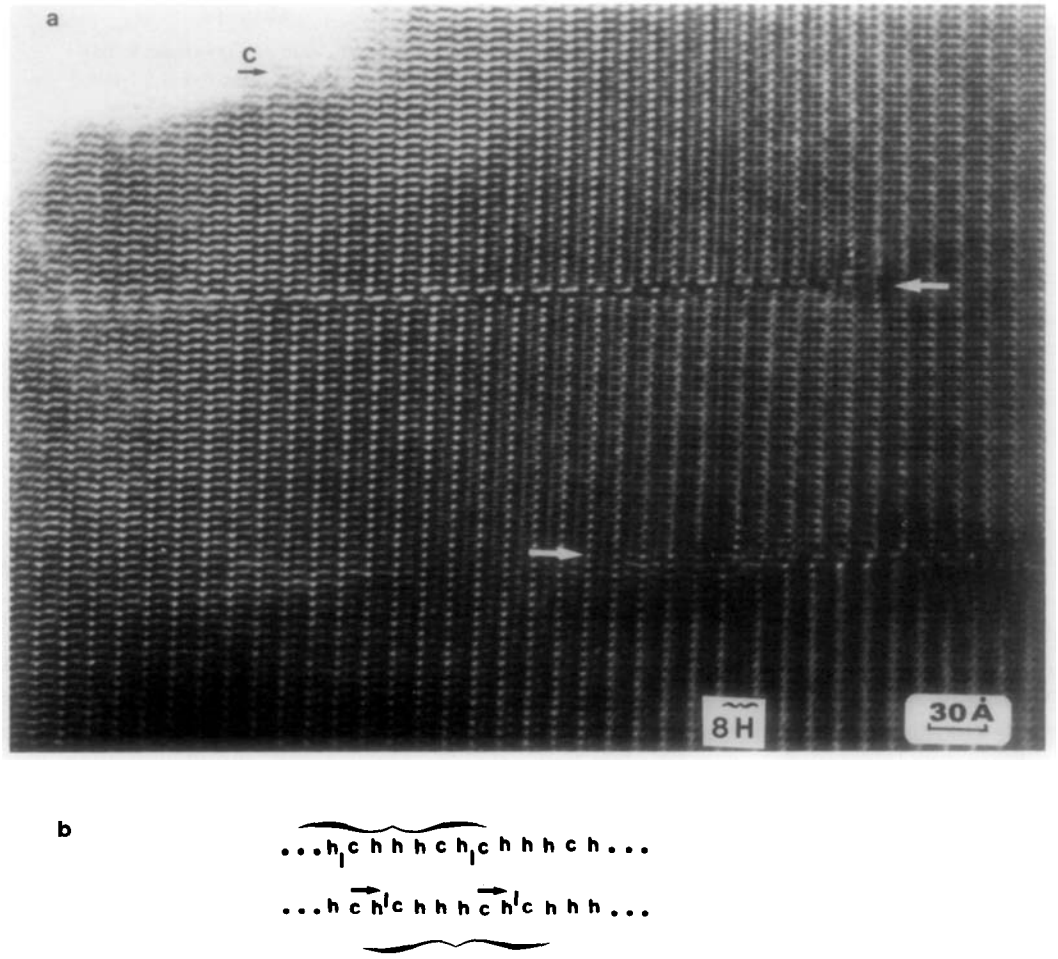

FIG. 6. An image of antiphase boundaries (a) with a schematic interpretation of the image (b).

(*20*). The other imperfection, rather rare, in the investigated crystals, was the occurrence of antiphase boundaries, such as shown in Fig. 6a; they are jagged boundaries, approximately normal to $[11\bar{2}0]$, with a displacement vector of $\frac{1}{3}$ **c** (schematic drawing is shown in Fig. 6b).

Structure of $BaMn_{1-x}Fe_xO_{3-\delta}$

It is thus confirmed that the BaO_3 layers are characterized in $BaMn_{1-x}Fe_xO_{3-\delta}$ oxides ($0 \leq x \leq 0.3$), by an unusual stacking sequence *hchhhc*, previously observed for $BaMnO_{2.90}$ (*3*) and called here 6H′. The structure of this oxide (Fig. 7) can be described in terms of two sorts of structural units M_4O_{15} built up from four face-sharing octahedra, and M_2O_9 units built up from two face-sharing octahedra. Along **c**, these strings of octahedra M_4O_{15} and M_2O_9 share their corners forming infinite ribbons.

The two principal original features which characterize this structure deal with the distribution of the manganese and iron atoms and the location of the oxygen vacancies in the structure. The preferential distribution

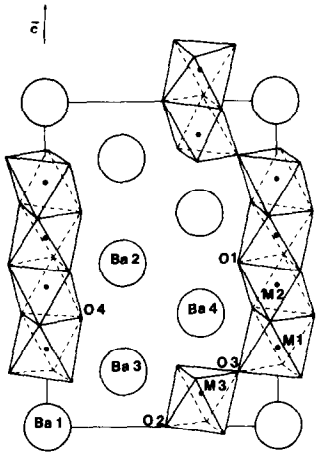

FIG. 7. Representation of the 6H′ structure following the c axis.

TABLE IV

FINAL R_I VALUES OBTAINED FROM DIFFERENT DISTRIBUTIONS OF THE MANGANESE (AND IRON) IONS

Distribution of Mn(%)			
*M*1	*M*2	*M*3	R_I factor
70.0	0.0	0.0	0.18
0.0	70.0	0.0	0.23
0.0	0.0	70.0	0.08
23.2	23.3	23.3	0.11
13.5	1.77	54.4	0.05

(Table III) involving manganese ions in the four face-sharing octahedra forming M_4O_{15} units, and iron atoms located in the two face-sharing octahedra of the M_2O_9 units, is remarkable. Moreover it can be observed that the iron content is smaller for the octahedra Oc_1 located at the center of the M_4O_{15} units (occupancy factor 2%) than for the octahedra Oc_2 located at the ends of these units (occupancy factor 10%). The validity of this distribution can easily be confirmed with Table IV which compares different distributions of the manganese and iron with the final results obtained from the refinements: a random distribution of the iron and manganese ions, as well as a preferential distribution of the iron atoms in the Oc_1 and Oc_2 octahedra would increase drastically the *R* factor and even a change of distribution between Oc_1 and Oc_2 would increase the *R* factor significantly. These results show clearly that the strings of four face-sharing octahedra M_4O_{15} are stabilized by the presence of manganese. Thus, it can now be predicted that structures such as 8H (Fig. 8a), or 15H (Fig. 8b) or 6H′ (Fig. 1), involving the presence of strings of four or five face-sharing octahedra will be favored by the presence of manganese, whereas cations such as iron will prefer structures such as 6H (Fig. 8c) involving only units of two face-sharing octahedra. The distribution of the oxygen vacancies is worth noting: the oxygen vacancies are found in the face-sharing positions of the M_2O_9 units whereas the M_4O_{15} units remain stoichiometric. These results are in agreement with the interatomic distances (Table V). The *M*–O distances in the Oc_1 and Oc_2 octahedra are very homogeneous, ranging from 1.904 to 1.948 Å; by contrast, the atoms located in the oxygen-deficient octahedra Oc_3 are strongly off-centered toward the fully occupied oxygen sites (i.e., cubic lay-

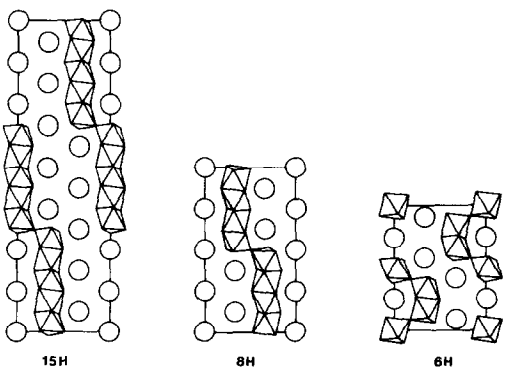

FIG. 8. Representation of the 8H (a), 15H (b), and the 6H (c) structures following the c axis.

TABLE V

INTERATOMIC DISTANCES FOR $BaMn_{0.767}Fe_{0.233}O_{2.87}$

Ba1–O2 : 2.853(2) Å	*M*1–*M*2 : 2.46(9) Å	O1–O1 : 2.593(28) Å
Ba1–O3 : 2.858(16)	*M*2–*M*2 : 2.352(78)	O1–O4 : 2.845(15)
Ba2–O1 : 2.847(1)		O2–O2 : 2.448(23)
Ba2–O4 : 3.007(14)	*M*1–O3 : 1.948(46)	O2–O3 : 2.825(17)
Ba3–O3 : 2.849(2)	*M*1–O4 : 1.930(53)	O3–O3 : 2.889(15)
Ba3–O4 : 2.786(29)	*M*2–O1 : 1.904(39)	O3–O3 : 2.798(15)
Ba4–O1 : 2.869(28)	*M*2–O4 : 1.946(39)	O3–O4 : 2.784(18)
Ba4–O3 : 2.898(30)	*M*3–O2 : 2.141(30)	O4–O4 : 2.593(24)
Ba4–O4 : 2.853(2)	*M*3–O3 : 1.829(20)	

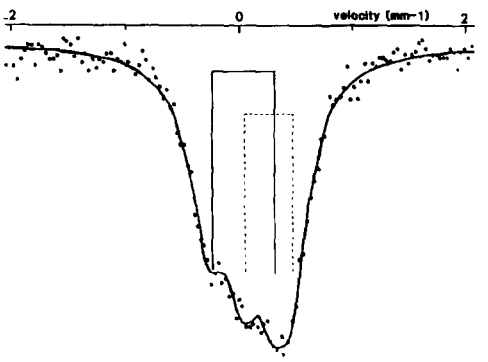

FIG. 9. Mössbauer spectrum of $BaMn_{0.766}Fe_{0.233}O_{2.87}$ compound at room temperature.

ers), with three short *M*–O distances (1.829 Å) and three long *M*–O distances (2.141 Å). This distribution of the oxygen vacancies in the M_2O_9 units seems to be characteristic of the manganese oxides: the compound 4H–$Ba_{0.5}Sr_{0.5}MnO_{2.84}$ (*10*) exhibits such a distribution. Nevertheless the latter oxide is only built up from M_2O_9 units and corner-sharing octahedra. Thus, the present results show the preferential distribution of the anionic vacancies in the M_2O_9 units, with respect to the M_4O_{15} built up from four face-sharing octahedra. The behavior of our 6H′ oxide is different from the one of the 6H–$BaFeO_{2.79}$ (4). In the latter oxide the oxygen vacancies are indeed distributed unequally between the face-sharing positions of the M_2O_9 units, i.e., in the hexagonal layers and the cubic layers (Fig. 8c). Thus it appears that the presence of manganese governs the distribution of the oxygen vacancies in the 6H′ structure of the oxide $BaMn_{0.766}Fe_{0.233}O_{2.87}$ in spite of the presence of iron.

Magnetic Study

To understand the distribution of the oxygen vacancies in this oxide a magnetic study and especially a Mössbauer investigation was necessary. The room-temperature Mössbauer spectrum (Fig. 9) shows that iron is present only in the trivalent state, leading to the formulation $Ba(Mn^{IV}Mn^{III})_{0.766}Fe^{III}_{0.233}O_{2.87}$. The variation of the magnetic susceptibility versus temperature (Fig. 10) from 4 to 600 K, confirms this formulation: the number of Bohr magnetons per mole $AMO_{2.87}$ $n = 4.76\ \mu_B$ is close to the theoretical value ($4.46\ \mu_B$). It is not possible to fit the Mössbauer spectrum without any ambiguity, owing to the great number of sites which are offered to Fe^{3+} in this structure. Nevertheless, the fitted values of the isomer shift and quadrupole splitting (Table VI) allow characterization of two sites for Fe^{3+} ions: one tetrahedral site with an occupancy factor of 54% and one octahedral site with an occupancy factor of 46%.

The creation of anionic vacancies in this structure can be explained by the formation

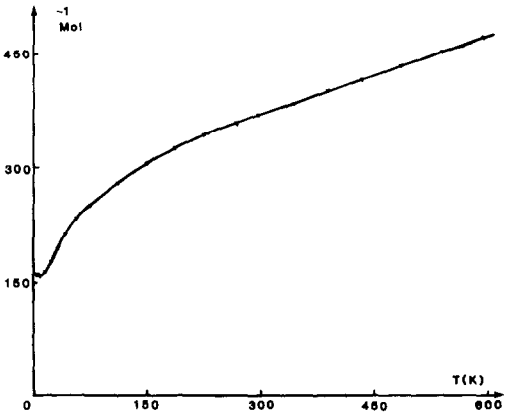

FIG. 10. Magnetic susceptibility versus temperature of the $BaMn_{0.766}Fe_{0.233}O_{2.87}$ compound.

TABLE VI

ROOM-TEMPERATURE MÖSSBAUER DATA OF $BaMn_{0.766}Fe_{0.233}O_{2.87}$

	Octahedral site	Tetrahedral site	
δ mm s^{-1}	0.38(1)	0.14(1)	
2ε mm s^{-1}	0.44(2)	0.58(2)	$Fe^{III}_{Oc}/Fe^{III}_{Oc+Te} = 0.46(5)$
Γ mm s^{-1}	0.36(2)	0.40(2)	

Note. δ, isomer shift relative to iron metal at room-temperature; 2ε, quadrupolar splitting; Γ, linewidth.

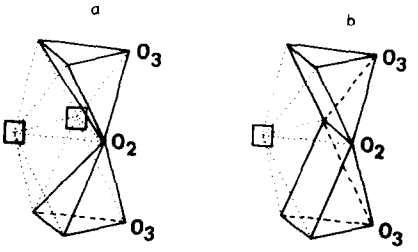

FIG. 11. (a) Creation of the FeO_4 tetrahedra in the two face-sharing octahedra. (b) Creation of the MnO_5 pyramid in the M_2O_9 unit.

of FeO_4 tetrahedra, and by the presence of MnO_5 trigonal or tetragonal pyramids. The FeO_4 tetrahedra result from the creation of two oxygen vacancies out of three oxygen sites of the two face-sharing octahedra (Fig. 11a) whereas the MnO_5 pyramids correspond to the creation of one oxygen vacancy out of three sites in the same M_2O_9 units (Fig. 11b); moreover, the latter polyhedra will only be observed for Mn^{3+} ions, owing to the Jahn-Teller properties of these species. From these considerations, it appears that one oxygen vacancy will be formed per Fe^{3+} ion in tetrahedral coordination, and one oxygen vacancy is possible for two Mn^{3+} ions in pyramidal coordination. Thus, if one assumes that all the Mn^{3+} ions exhibit a pyramidal coordination, the distributions of the different ions deduced from the neutron diffraction data and Mössbauer spectroscopy would lead to the following structural formulation:

$$Ba_6[(Fe^{3+}_{0.035}Mn^{4+}_{1.965})_{Oc_1}(Fe^{3+}_{0.27}Mn^{4+}_{1.73})_{Oc_2}]^{M_4O_{15}}$$
$$[(Mn^{3+}_{0.10})_{pyr}(Fe^{3+}_{0.752})_{tet.}(Mn^{4+}_{0.812})_{Oc_3}$$
$$(Fe^{3+}_{0.336})_{Oc_3}]^{M_2O_9}O_{17.19}$$

The calculated value of the oxygen content 17.19, which does not take into account the electroneutrality, is in agreement with the experimental value 17.23. The difference between these values can easily be explained not only by the experimental errors in the chemical analysis, but also mainly by the lack of accuracy in the distribution obtained from the Mössbauer observation. Moreover, it is also possible that a part of the Mn^{3+} ions would assume an octahedral coordination.

However, it must be pointed out that the ability of the Mn^{3+} ions to create oxygen vacancies by forming edge-sharing MnO_5 pyramids from the "Mn_2O_9" units is demonstrated by the existence of the 6H′ $BaMnO_{3-x}$ oxides. If one considers the mechanism described in Fig. 11b, the most oxygen-deficient oxide characterized by planes of edge-sharing MnO_5 pyramids sharing their corners with "M_4O_{15}" units would correspond to $x_1 = \frac{1}{6}$, i.e., a number of Mn^{3+} ions in the pyramidal planes $n_1 = 2x_1 = \frac{1}{3}$ in the formulation $BaMnO_{3-x}$. This model is in very good agreement with the most oxygen-deficient oxide 6H′–$BaMn^{III}_{0.30}Mn^{IV}_{0.70}O_{2.85}$ observed by Negas and Roth (*3*).

A systematic structural investigation of the substitution of iron for manganese in the $BaMnO_{3-x}$ oxides, by neutron diffraction HREM and Mössbauer spectroscopy should permit the problem of oxygen deficiency in those compounds to be understood.

Acknowledgments

The authors are grateful to Dr. J. M. Grenèche, Université du Maine, for helpful discussion in the Mössbauer study.

References

1. L. KATZ AND R. WARD, *Inorg. Chem.* **3,** 205 (1964).
2. "International Tables for X-Ray Crystallography," Vol. II, p. 342, Kynoch Press, Birmingham, 1959.
3. T. NEGAS AND R. S. ROTH, *J. Solid State Chem.* **3,** 323 (1971).
4. A. J. JACOBSON, *Acta Crystallogr. Sect. B* **32,** 1087 (1976).
5. M. ZANNE ET G. GEITZER, *Bull. Soc. Chim. Fr.* **5,** 1568 (1971).
6. M. ZANNE, A. COURTOIS, AND C. GLEITZER, *Bull. Soc. Chim. Fr.,* 4470 (1972).
7. T. NEGAS AND R. S. ROTH, BS Special Publication 364, 1972.
8. A. J. JACOBSON AND J. L. HUTCHISON, *J. Solid State Chem.* **35,** 334 (1980).
9. B. L. CHAMBERLAND, A. W. SLEIGHT, AND J. F. WEIMER, *J. Solid State Chem.* **1,** 506 (1970).
10. A. J. JACOBSON AND A. J. W. HORROX, *Acta Crystallogr. Sect. B* **32,** 1003 (1976).
11. R. D. BURBANK AND M. T. EVANS, *Acta Crystallogr.* **1,** 330 (1948).
12. B. L. CHAMBERLAND, *Inorg. Chem.* **8,** 286 (1969).
13. J. L. HUTCHISON AND J. S. ANDERSON, *Electron Microsc. Anal.,* 301 (1977).
14. J. L. HUTCHISON AND A. J. JACOBSON, *J. Solid State Chem.* **20,** 417 (1977).
15. J. L. HUTCHISON, *Chem. Scripta* **14,** 181 (1978).
16. J. L. HUTCHISON AND A. J. JACOBSON, *Acta Crystallogr. Sect. B* **31,** 1442 (1975).
17. J. L. HUTCHISON AND D. J. SMITH, *Acta Crystallogr. Sect. A* **37,** 119 (1981).
18. P. L. GAI, A. J. JACOBSON AND C. N. RAO, *Inorg. Chem.* **15,** 2, 481 (1976).
19. A. J. SKARNULIS, E. SUMMERVILLE, AND L. EYRING, *J. Solid State Chem.* **23,** 59 (1978).
20. A. POTOFF, B. L. CHAMBERLAND, AND L. KATZ, *J. Solid State Chem.* **8,** 234 (1973).
21. J. TEILLET AND F. VARRET, Laboratoire de Spectrométrie Mössbauer, Université du Maine, Le Mans, France.